International Tables for Crystallography (2018). Vol. H, Section 2.5.4.4, pp. 145–147.

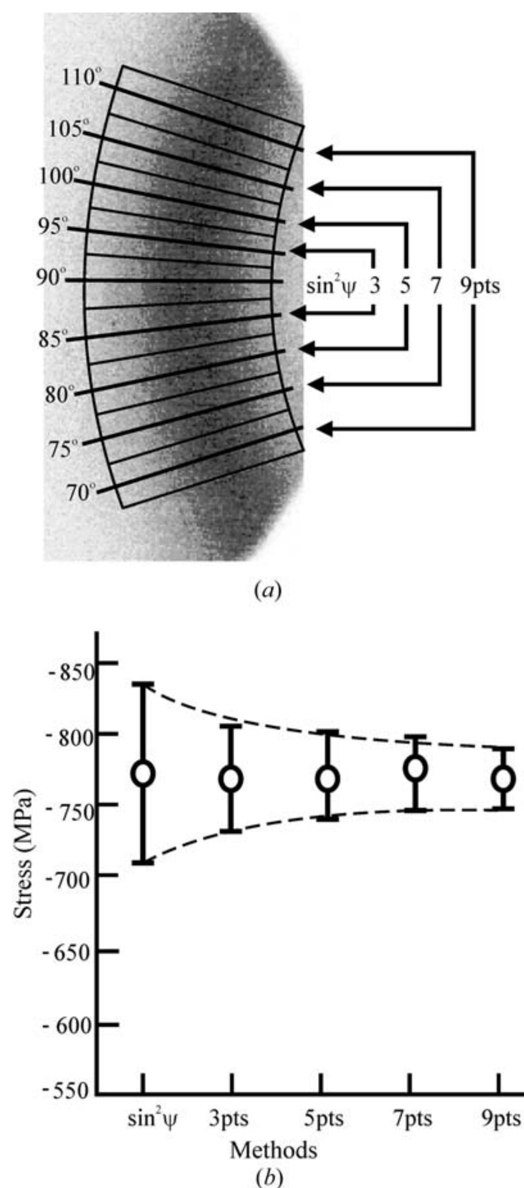

Figure 2.5.27
Stress calculation with the 2D method and the $\sin^2\psi$ method: (*a*) nine data points (abbreviated as pts) on the diffraction ring; (*b*) measured stress and standard deviation by different methods.

dimensional diffraction system, more crystallites can contribute to the diffraction because of the larger γ range.

An example of a stress calculation is provided by the measurement of the residual stress on the end surface of a carbon steel roller. One of the seven frames taken with an ω scan is shown in Fig. 2.5.27(*a*). The (211) ring covering the γ range 67.5 to 112.5° was used for stress analysis. First, the frame data were integrated along γ with an interval of $\Delta\gamma$ = 5°. A total of nine diffraction profiles were obtained from γ integration. The peak position 2θ for each γ angle was then obtained by fitting the profile with a Pearson-VII function. A total of 63 data points can be obtained from the seven frames. The data points at γ = 90° from seven frames, a typical data set for an ω diffractometer, were used to calculate the stress with the conventional $\sin^2\psi$ method. In order to compare the gain from having increased data points with the 2D method, the stress was calculated from 3, 5, 7 and 9 data points on each frame. The results from the conventional $\sin^2\psi$ method and the 2D method are compared in Fig. 2.5.27(*b*). The measured residual stress is compressive and the stress values from different methods agree very well. With the data taken from the same measurement (seven frames), the 2D method gives a lower standard error and the error decreases with increasing number of data points from the diffraction ring.

2.5.4.4. *Quantitative analysis*

2.5.4.4.1. *Crystallinity*

The crystallinity of a material influences many of its characteristics, including mechanical strength, opacity and thermal properties. Crystallinity measurement provides valuable information for both materials research and quality control in materials processing. The diffraction pattern from a material containing both amorphous and crystalline solids has a broad feature from the amorphous phase and sharp peaks from the crystalline phase. The weight percentage of the crystalline phases in a material containing both crystalline and amorphous phases can be determined by X-ray diffraction (Chung & Scott, 1973; Alexander, 1985; Murthy & Barton, 2000; Kasai & Kakudo, 2005). Assuming that the X-ray scattering intensity from each phase in such a material is proportional to its weight percentage, and that the scattering intensities from all phases can be measured within a given 2θ range, the per cent crystallinity is given by

$$x_{\rm pc} = 100\% \frac{I_{\rm crystal}}{I_{\rm crystal} + I_{\rm amorphous}}, \qquad (2.5.90)$$

where $x_{\rm pc}$ is the per cent crystallinity, $I_{\rm crystal}$ is the integrated intensity of all crystalline peaks and $I_{\rm amorphous}$ is the integrated intensity of the amorphous scattering. The accuracy of the measured per cent crystallinity depends on the integrated diffraction profile. Since most crystalline samples have a preferred orientation, it is very difficult to obtain a consistent measurement of crystallinity with a conventional diffractometer. Fig. 2.5.28 shows a 2D diffraction frame collected from an oriented polycrystalline sample. The diffraction is in transmission mode with the X-ray beam perpendicular to the plate sample surface. Fig. 2.5.28(*a*) shows a diffraction profile integrated from a horizontal region analogous to a profile collected with a conventional diffractometer. Only one peak from the crystalline phase can be observed in the profile. It is also possible that a different peak or no peak is measured if the sample is loaded in other orientations. Fig. 2.5.28(*b*) is the diffraction profile integrated from the region covering all peaks from the crystalline phase over almost all azimuthal angles. A total of four peaks from the crystalline phase are observed. This shows that a 2D-XRD system can measure per cent crystallinity more accurately and with more consistent results (Pople *et al.*, 1997; Bruker, 2000) than a conventional system.

2.5.4.4.2. *Crystallite size*

The size of the crystallites in a polycrystalline material has a significant effect on many of its properties, such as its thermal, mechanical, electrical, magnetic and chemical properties. X-ray diffraction has been used for crystallite-size measurement for many years. Most methods are based on diffraction-line broadening and line-profile analysis (Wilson, 1971; Klug & Alexander, 1974; Ungár, 2000). Another approach to crystallite-size measurement is based on the spotty diffraction rings collected with two-dimensional detectors when a small X-ray beam is used (Cullity, 1978; He, 2009). Line-profile analysis is based on the diffraction profile in the 2θ direction, while crystallite-size analysis with a spotty 2D diffraction pattern is based on the diffraction profile in the γ direction. The latter may be referred to as γ-profile analysis.

Copyright © 2018 International Union of Crystallography

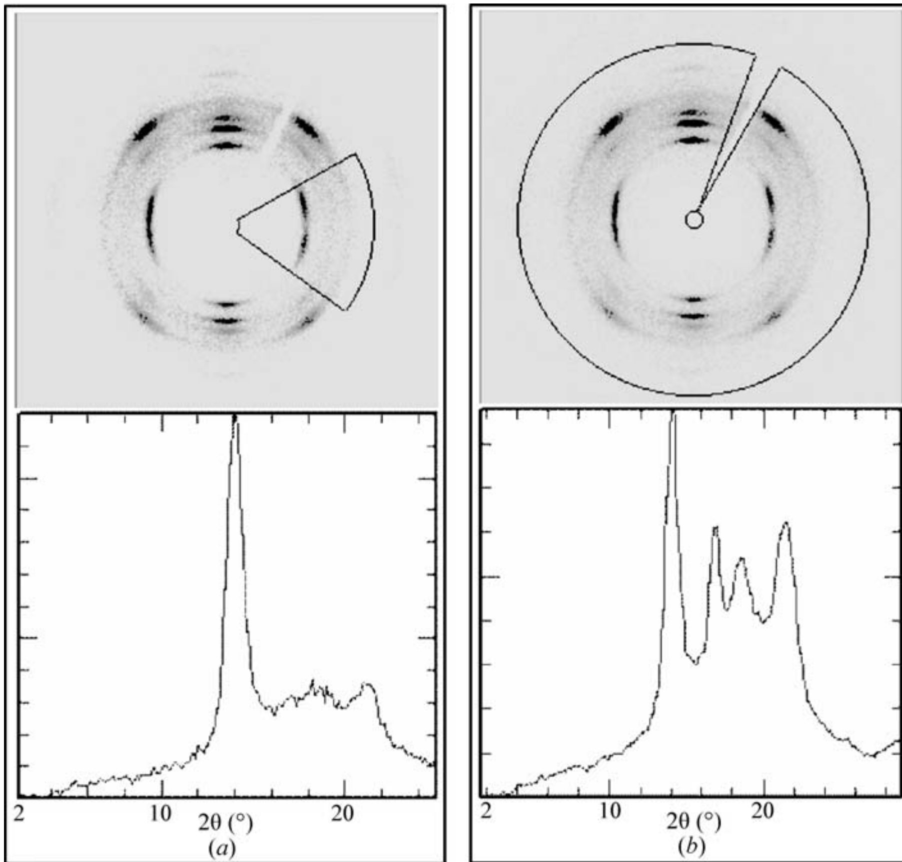

Figure 2.5.28
2D diffraction pattern from an oriented polycrystalline polymer sample. (*a*) Diffraction profile integrated from a horizontal region analogous to a profile collected with point detector. (*b*) Diffraction profile integrated from all parts of the 2D frame.

Fig. 2.5.29(*a*) shows a diffraction profile collected from gold nanoparticles and regular gold metal. The 2θ profile from the gold nanoparticles is significantly broader than the profile from regular gold metal. The crystallite size can be calculated by measuring the broadening and using the Scherrer equation:

$$B = \frac{C\lambda}{t\cos\theta}, \qquad (2.5.91)$$

where λ is the X-ray wavelength (in Å), B is the full width at half maximum (FWHM) of the peak (in radians) corrected for instrumental broadening and strain broadening, θ is the Bragg angle, C is a factor, typically from 0.9 to 1.0, depending on the crystallite shape (Klug & Alexander, 1974), and t is the crystallite size (also in Å). This equation shows an inverse relationship between crystallite size and peak-profile width. The wider the peak is, the smaller the crystallites. The 2θ diffraction profiles can be obtained either by using a conventional diffractometer with a point or line detector, or by γ integration from a diffraction pattern collected with 2D detector. When a 2D detector is used, a long sample-to-detector distance should be used to maximize the resolution. A small beam size and low convergence should also be used to reduce instrument broadening.

Fig. 2.5.29(*b*) shows a frame collected from an SRM660a (LaB_6) sample with a 2D-XRD system. The spotty diffraction rings are observed with average crystallite size of 3.5 µm. The number of spots in each diffraction ring is determined by the crystallite size and diffraction volume. Introducing a scaling factor covering all the numeric constants, the incident-beam divergence and the calibration factor for the instrument, we obtain an equation for the crystallite size as measured in reflection mode:

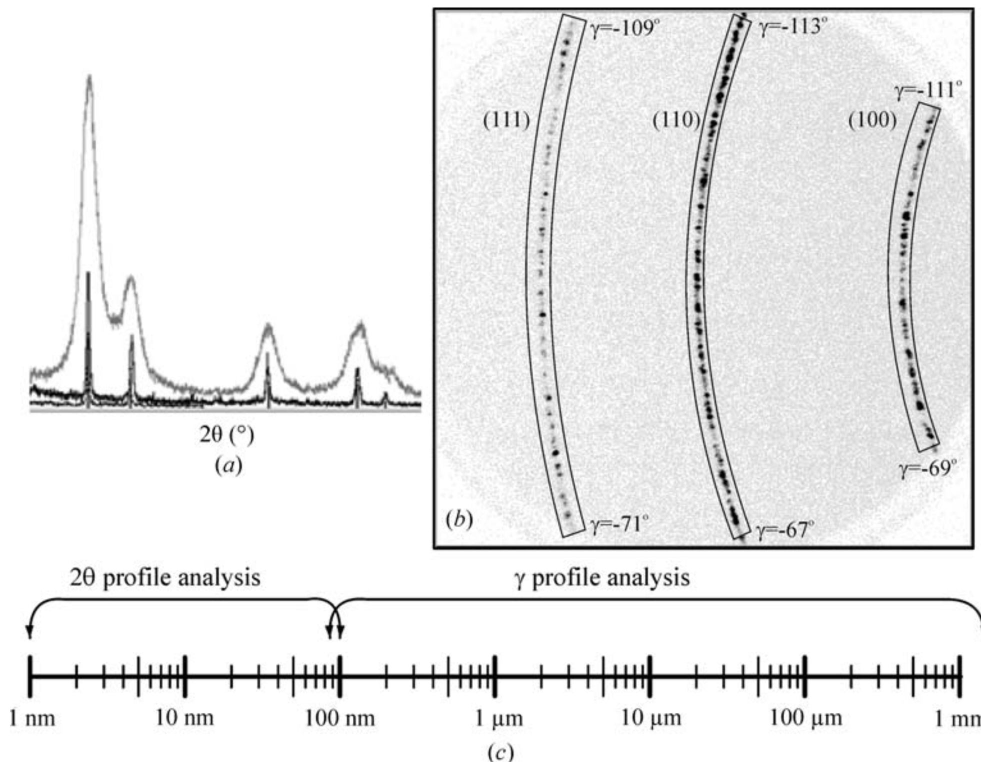

Figure 2.5.29
Crystallite-size analysis: (*a*) 2θ profile of a gold nanoparticle (grey) and regular gold metal (black); (*b*) γ profile of LaB_6; (*c*) measurement range.

$$d = k\left\{\frac{p_{hkl}b^2 \arcsin[\cos\theta\sin(\Delta\gamma/2)]}{\mu N_s}\right\}^{1/3}, \qquad (2.5.92)$$

where d is the diameter of the crystallite particles, p_{hkl} is the multiplicity of the diffracting planes, b is the size of the incident beam (*i.e.* its diameter), $\Delta\gamma$ is the γ range of the diffraction ring, μ is the linear absorption coefficient and N_s is the number of spots within $\Delta\gamma$. For transmission mode, we have

$$d = k\left\{\frac{p_{hkl}b^2 t \arcsin[\cos\theta\sin(\Delta\gamma/2)]}{N_s}\right\}^{1/3}, \qquad (2.5.93)$$

where t is the sample thickness. In transmission mode with the incident beam perpendicular to the sample surface, the linear absorption coefficient affects the relative scattering intensity, but not the actual sampling volume. In other words, all the sample volume irradiated by the incident beam contributes to the diffraction. Therefore, it is reasonable to ignore the absorption effect $\exp(\mu t)$ for crystallite-size analysis as long as the sample is thin enough for transmission-mode diffraction. The effective sampling volume reaches a maximum for transmission-mode diffraction when $t = 1/\mu$.

For both reflection and transmission,

$$k = \left(\frac{3\beta}{8\pi}\right)^{1/3}, \qquad (2.5.94)$$

where β is the divergence of the incident beam. Without knowing the precise instrumental broadening, k can be treated as a calibration factor determined from the 2D diffraction pattern of a known standard. Since only a limited number of spots along the diffraction ring can be resolved, it can be seen from equation (2.5.94) that a smaller X-ray beam size and low-multiplicity peak should be used if a smaller crystallite size is to be determined.

Fig. 2.5.29(c) shows the measurement ranges of 2θ-profile and γ-profile analysis. The 2θ-profile analysis is suitable for crystallite sizes below 100 nm (1000 Å), while γ-profile analysis is suitable for crystallite sizes from as large as tens of µm down to 100 nm with a small X-ray beam size. By increasing the effective diffraction volume by translating the sample during data collection or multiple sample integration (or integrating data from multiple samples), the measurement range can be increased up to millimetres. Multiple sample integration can deal with large crystallite sizes without recalibration. The new calibration factor is given as

$$k_n = n^{1/3}k, \qquad (2.5.95)$$

where n is the number of targets that are integrated. The number of crystallites can be counted by the number of intersections of the γ profile with a threshold line. Every two intersections of the γ profile with this horizontal line represents a crystallite. In order to cancel out the effects of preferred orientation and other material and instrumental factors on the overall intensity fluctuation along the γ profile, one can use a trend line fitted to the γ profile by a second-order polynomial. It is always necessary to calibrate the system with a known standard, preferably with a comparable sample geometry and crystallite size. For reflection mode, it is critical to have a standard with a comparable linear absorption coefficient so as to have similar penetration.

References

Alexander, L. E. (1985). *X-ray Diffraction Methods in Polymer Science*. Malabar: Krieger Publishing Company.

Allahkarami, M. & Hanan, J. C. (2011). *X-ray diffraction mapping on a curved surface*. *J. Appl. Cryst.* **44**, 1211–1216.

Arndt, U. W. (1986). *X-ray position-sensitive detectors*. *J. Appl. Cryst.* **19**, 145–163.

Arndt, U. W. (1990). *Focusing optics for laboratory sources in X-ray crystallography*. *J. Appl. Cryst.* **23**, 161–168.

Bergese, P., Bontempi, E., Colombo, I. & Depero, L. E. (2001). *Micro X-ray diffraction on capillary powder samples: a novel and effective technique for overcoming preferred orientation*. *J. Appl. Cryst.* **34**, 663–665.

Bhuvanesh, N. S. P. & Reibenspies, J. H. (2003). *A novel approach to micro-sample X-ray powder diffraction using nylon loops*. *J. Appl. Cryst.* **36**, 1480–1481.

Birkholz, M. (2006). *Thin Film Analysis by X-ray Scattering*, pp. 191–195. Weinheim: Wiley-VCH.

Blanton, T. N. (1994). *X-ray diffraction orientation studies using two-dimensional detectors*. *Adv. X-ray Anal.* **37**, 367–373.

Blanton, T. N. (2003). *X-ray film as a two-dimensional detector for X-ray diffraction analysis*. *Powder Diffr.* **18**, 91–98.

Bloomer, A. C. & Arndt, U. W. (1999). *Experiences and expectations of a novel X-ray microsource with focusing mirror. I*. *Acta Cryst.* D**55**, 1672–1680.

Boesecke, P. (2007). *Reduction of two-dimensional small- and wide-angle X-ray scattering data*. *J. Appl. Cryst.* **40**, s423–s427.

Bontempi, E., Benedetti, D., Massardi, A., Zacco, A., Borgese, L. & Depero, L. E. (2008). *Laboratory two-dimensional X-ray microdiffraction technique: a support for authentication of an unknown Ghirlandaio painting*. *Appl. Phys. A*, **92**, 155–159.

Borgonovi, G. M. (1984). *Determination of residual stress from two-dimensional diffraction pattern*. *Nondestructive Methods for Material Property Determination*, edited by C. O. Ruud & R. E. Green Jr, pp. 47–57. New York: Plenum Publishing Corporation.

Bourgeois, D., Moy, J. P., Svensson, S. O. & Kvick, Å. (1994). *The point-spread function of X-ray image-intensifiers/CCD-camera and imaging-plate systems in crystallography: assessment and consequences for the dynamic range*. *J. Appl. Cryst.* **27**, 868–877.

Bruker (2000). *Percent crystallinity in polymer*. Bruker AXS Lab Report No. L86-E00005.

Bunge, H. J. (1983). *Texture Analysis in Materials Science*. London: Butterworth.

Bunge, H. J. & Klein, H. (1996). *Determination of quantitative, high-resolution pole-figures with the area detector*. *Z. Metallkd.* **87**(6), 465–475.

Campbell, J. W., Harding, M. M. & Kariuki, B. (1995). *Spatial-distortion corrections, for Laue diffraction patterns recorded on image plates, modelled using polynomial functions*. *J. Appl. Cryst.* **28**, 43–48.

Cervellino, A., Giannini, C., Guagliardi, A. & Ladisa, M. (2006). *Folding a two-dimensional powder diffraction image into a one-dimensional scan: a new procedure*. *J. Appl. Cryst.* **39**, 745–748.

Chung, F. H. & Scott, R. W. (1973). *A new approach to the determination of crystallinity of polymers by X-ray diffraction*. *J. Appl. Cryst.* **6**, 225–230.

Cullity, B. D. (1978). *Elements of X-ray Diffraction*, 2nd ed. Reading, MA: Addison-Wesley.

Derewenda, Z. & Helliwell, J. R. (1989). *Calibration tests and use of a Nicolet/Xentronics imaging proportional chamber mounted on a conventional source for protein crystallography*. *J. Appl. Cryst.* **22**, 123–137.

Dickerson, M. B., Pathak, K., Sandhage, K. H., Snyder, R. L., Balachandran, U., Ma, B., Blaugher, R. D. & Bhattacharya, R. N. (2002). *Applications of 2D detectors in x-ray analysis*. *Adv. X-ray Anal.* **45**, 338–344.

Durst, R. D., Carney, S. N., Diawara, Y. & Shuvalov, R. (2002). *Readout structure and technique for electron cloud avalanche detectors*. US Patent No. 6, 340, 819.

Eatough, M. O., Rodriguez, M. A., Blanton, T. N. & Tissot, R. G. (1997). *A comparison of detectors used for microdiffraction applications*. *Adv. X-ray Anal.* **41**, 319–326.

Ercan, A., Tate, M. W. & Gruner, S. M. (2006). *Analog pixel array detectors*. *J. Synchrotron Rad.* **13**, 110–119.